Advanced Optical Materials

ADVANCED OPTICAL MATERIALS
www.advopticalmat.de

RESEARCH ARTICLE OPEN ACCESS

Design of Molecular Lanthanide-Based Quantum Light Sources for On-Chip Integration

Silvia Bonabello[1] | Rodolpho Alessandro Nesta Silva[1] | Dimitrije Mara[1] | Fabio Travagin[2] | Marzia Petreti[2] | Marco Saccone[3] | Matteo Melegari[4] | Luciano Marchiò[4] | Luca Pilia[5] | Giovanni Battista Giovenzana[2] | Flavia Artizzu[1]

[1]LumiMol Lab – Dipartimento per Lo Sviluppo Sostenibile e La Transizione Ecologica, Università del Piemonte Orientale, Vercelli, Italy | [2]Dipartimento di Scienze del Farmaco, Università del Piemonte Orientale, Novara, Italy | [3]Dipartimento di Scienze e Innovazione Tecnologica, Università del Piemonte Orientale, Alessandria, Italy | [4]Dipartimento Di Scienze Chimiche, della Vita e della Sostenibilità Ambientale, Università di Parma, Parma, Italy | [5]Dipartimento di Ingegneria Meccanica Chimica e dei Materiali, Università di Cagliari, Cagliari, Italy

Correspondence: Flavia Artizzu (flavia.artizzu@uniupo.it)

Received: 1 December 2025 | **Revised:** 2 February 2026 | **Accepted:** 13 February 2026

Keywords: europium emission | lanthanide-doped films | lanthanides | luminescence | quantum light sources

ABSTRACT

Lanthanide-based optical emitters are emerging as promising materials for quantum applications because of the long optical coherent lifetimes associated with their narrow emission lines. In this work, we investigate a series of lanthanide molecular complexes with a highly rigid tetrapodal benzimidazolic ligand (**L**) as potential highly coherent quantum light sources suitable for on-chip integration. The **LnL** complexes show sensitized Ln-centered emission in the visible and near-infrared spectral ranges with a well-resolved fine structure of the *J* sublevels. Remarkably, the **EuL** complex exhibits a single line related to the purely electric dipole $^5D_0 \rightarrow {}^7F_0$ transition, of particular interest in quantum photonics. Notably, this formally forbidden line likely originates from an LMCT state, rather than from low symmetry or strong crystal-field effects. This mechanism enables the appearance of the band while maintaining a limited electric inhomogeneity of the ligand system, as supported by Judd–Ofelt analysis. These features contribute to the significant reduction of the room-temperature inhomogeneous linewidth (~500 GHz) compared to typical zero-phonon lines of polyaromatic molecules in polymers. Importantly, these favorable properties persist in doped silica-based SiCO and PMMA films. Additionally, the doped SiCO film provides high excitation selectivity, minimal host autofluorescence, and broad color tunability.

1 | Introduction

Quantum photonic technologies represent the future paradigm for efficient data communication, computing, information storage, cybersecurity, and sensing [1]. Novel sources of quantum light, offering optical properties modulation by chemical engineering together with the flexibility for on-chip integration in quantum devices, are highly sought after to overcome the limits imposed by traditional inorganic materials, such as bulky crystals and quantum dots [1, 2]. In this context, single molecules are particularly promising as quantum emitters as they can provide competitive performance in terms of coherence, scalability, and compatibility with diverse integrated platforms [3]. Moreover, chemical tailoring at the atomic and molecular scale can open novel opportunities for the control of the interactions between quantum systems (e.g., nuclear spins) and light, as well as simultaneously engineer the quantum properties of photons [4–7]. This can be achieved by exploiting the intrinsically well-defined transition electric (and magnetic) dipole moments in molecules, allowing for optically narrow linewidths, typically

corresponding to zero-phonon lines, and long coherence lifetimes of the emitted light. Single organic molecules, mostly belonging to the class of polyaromatic hydrocarbons, are currently attracting much interest as quantum emitters due to their accessibility, large quantum yields, and their high rigidity, resulting in well-aligned ground and upper states and therefore enhanced zero-phonon lines [8–11]. Increasing the rigidity of the system, leveraging on the high purity and structural definition of molecular materials, and embedding them as dopants into suitable hosts, can lead to significant control of the inhomogeneous broadening of lines due to phonon states even out of cryogenic temperatures [12–14]. In addition, the incorporation of such quantum sources in dielectric media is necessary to allow their combination with metal mirror cavities for signal enhancement while avoiding plasmon quenching caused by the direct contact of the emitter with the metal surface [15]. However, the optical tunability and the physical and chemical versatility (e.g., wavelength modulation, multifunctionality, solubility, compatibility with various photonic chip platforms) of polyaromatic hydrocarbons are highly limited. In this framework, luminescent lanthanide (Ln)-based molecular complexes with organic ligands can represent an empowered class of quantum light sources, leveraging on the enhanced chemical versatility from ligand modification and the unique optical properties of trivalent Ln ions (Ln^{3+}). Indeed, Ln emission lines, stemming from intra-shell transitions essentially involving core-like 4*f* orbitals, are barely influenced by the external environment, intrinsically narrow, unaffected by spectral diffusion, and characterized by long optical coherence lifetimes [4–7, 16–18]. In molecular Ln complexes, the organic ligand acts as a sensitizing antenna, able to harvest light with high efficiency and transfer it directly to the Ln emitter. This mechanism allows overcoming the intrinsically weak absorption of the Ln emitters, enabling efficient optical pumping and the on-demand control of photon emission [19]. Furthermore, their high chemical versatility allows for finely tailoring the Ln optical properties by modulating the local symmetry and ligand field effects influencing orbital mixing and transition lines splitting, intensity, and width [20, 21]. The design of Ln-based molecular quantum light sources requires the use of organic ligands suitable to bestow high rigidity to the molecular structure to minimize phonon-mediated relaxation pathways and reduce inhomogeneous line broadening. At the same time, a rigid ligand system introduces symmetry constraints that can affect the oscillator strengths of selected Ln-centered transitions, which obey electric or magnetic (or mixed) dipole selection rules, making the rational design of such quantum emitters a challenging task. The investigation of Ln molecular complexes as quantum light sources, which can open wide, so far largely unexplored, opportunities for even more sophisticated quantum systems, for example optical-spin polarization [4], has only emerged in the last few years, whereas currently available research is mostly focused on fully inorganic materials [17]. Therefore, more extended studies are highly demanded to improve the understanding of how to control the quantum states of Ln emitters by molecular engineering, and how these features respond to modifications of the chemical surroundings when the emitter is incorporated into matrices suitable for on-chip integration.

In this work, we present an in-depth investigation of the structure-properties relationship of a class of Ln ions (Ln = Eu, Tb, Sm, Gd, Nd, Er, Yb) complexes with the neutral tris((1H-benzo[d]imidazol-2-yl)methyl)amine ligand (**L**) showing sensitized optical Ln-centered emission in the visible and near-infrared (NIR) spectral ranges. The tris-benzimidazolic **L** ligand has been selected for its optical properties of UV absorber, able to undergo energy transfer to Ln ions with high-lying emitting levels, such as Eu and Tb, and for its ability to coordinate the metal ions in a highly rigid tetrapodal fashion [22, 23], resulting in remarkably well-resolved Ln-centered emission lines in the **LnL** complexes. To explore the potential of the synthesized compounds for on-chip integrated quantum light sources, they were incorporated into suitable transparent and flexible silica-based thin films, obtained from natural chemical precursors, representing the ideal dielectric medium for the combination with metal optical cavities. We highlight the role of symmetry, ligand-metal interaction, and rigidity of the system, on the emission lines of the Ln ions, particularly focusing on the influence of different phases (solution, crystalline state and doped transparent films) on the spectral properties of Eu^{3+}, the most promising quantum light emitter in relation to its purely electric dipolar $^5D_0 \rightarrow {}^7F_0$ transition [4–6], giving rise to emission at 580 nm. Remarkably, we found that this transition is governed by low-lying charge transfer states rather than the commonly accounted mixing of *J*-levels induced by strong crystal field effects and low symmetry, with important consequences on the inhomogeneous linewidth in both the single crystals and in the doped films. The discussed results can provide novel guidelines for the rational design of Ln-based single-molecule quantum emitters that are integrable on photonic platforms. Finally, we show that **EuL** and **TbL**-doped hybrid silica films display remarkable, highly selective wavelength-dependent emission color tunability suitable for applications not only in quantum photonics, but also in optical multiplexing and anticounterfeiting.

2 | Results and Discussion

2.1 | Synthesis and Crystal Structure Description

LnL complexes (Ln = Nd, Sm, Eu, Gd, Tb, Er, Yb) were synthesized though a one-pot reaction by directly adding a solution in ethanol (EtOH) of the appropriate Ln nitrate salt to a solution of the ligand **L** in the same solvent at room temperature which yielded the immediate precipitation of the complexes as white microcrystalline powders (Figure 1). Prismatic single crystals suitable for structural investigation by X-ray diffraction (scXRD) were obtained for **EuL** and **TbL** by slow diffusion of the Ln ion-containing solution into the solution of the ligand **L** in EtOH. The compounds crystallize in the cubic Pa-3 space group, and the molecular arrangement consists of a mononuclear complex which can be formulated $[LnL(NO_3)_3]$, where the trivalent Ln ion is coordinated by one **L** ligand and three nitrate ions, in agreement with previous reports [22, 23]. The molecular structure of **EuL** is depicted in Figure 2a as a representative example, while the structure of the Tb^{3+} analog is reported in Supporting Information together with crystallographic data (Figure S4 and Table S1). In the mononuclear unit, the central trivalent Ln ion is deca-coordinated through four N-donor atoms (three of the imidazolic units and one of the aminogroup) of the **L** ligand acting as tetrapodal chelator, and six O-donor atoms by three nitrate ions, adopting a distorted bicapped square antiprism geometry (D_{4d}, Figure 2b) as confirmed by continuous shape

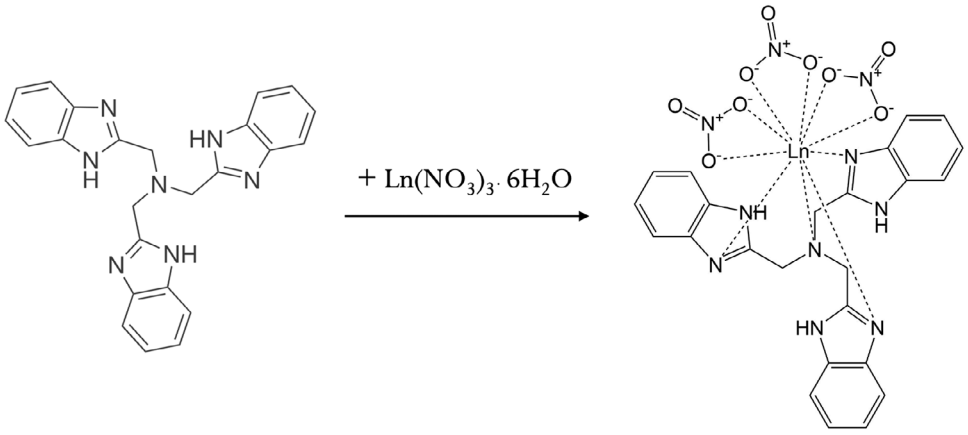

FIGURE 1 | General reaction scheme for the synthesis of **LnL** complexes.

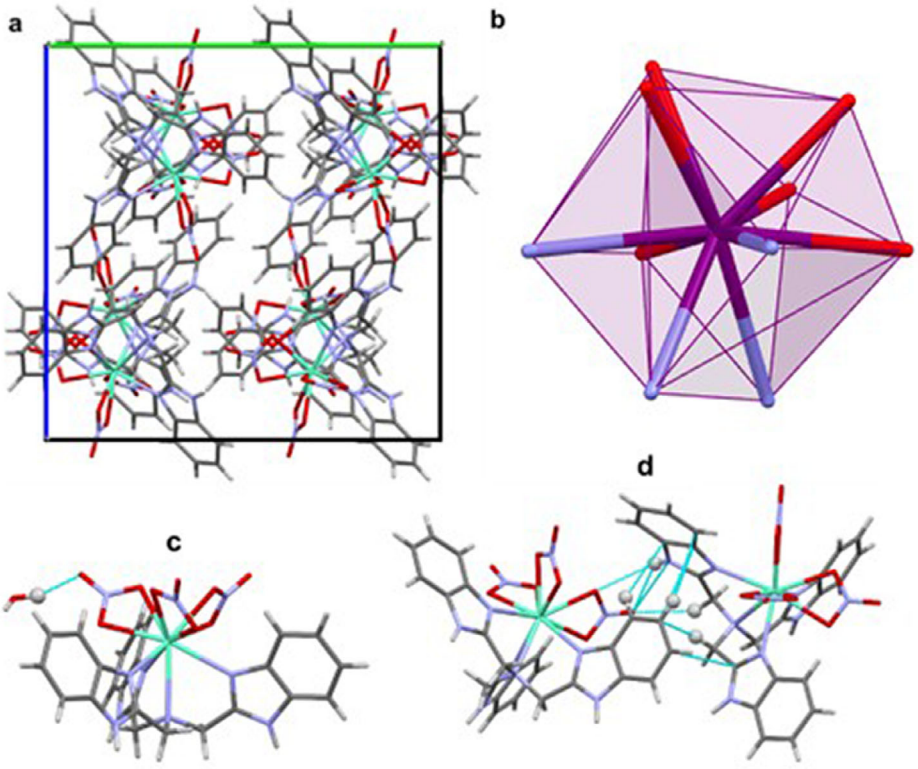

FIGURE 2 | (a) Capped stick representation of the unit cell of **EuL** (view along the *a*-axis) in which the partially disordered water is omitted for clarity. (b) Coordination geometry of the Ln^{3+} ion. (c) Capped stick representation of the **EuL**-water dimer. (d) Capped stick representation of the **EuL**-**EuL** dimer. Hanging hydrogens are represented as balls. Color codes: light blue, Eu; red, O; blue, N; gray, C; white, H.

analysis (Tables S2 and S3). When considering the inequivalence of the N and O donor atoms, the local symmetry around the Ln center lowers to C_3 (see Supporting Information for details). All the **LnL** complexes herein investigated are isostructural, as confirmed by powder-XRD (pXRD, Figure S5) and FT-IR (Figure S6) data. Thermogravimetric investigation indicates that the complexes are stable up to 300°C (Figure S7), suggesting that they are suitable for integration into hybrid systems through functional processing or material transformation.

It is well known that the intermolecular interaction pattern influences crystal packing and can drive the formation of supramolecular structures with desired shape and functions [24]. In this respect, several interesting noncovalent interactions occur in the complexes. First, the complexes include a solvated water molecule, which, although partially disordered, is hydrogen bonded to one of the noncomplexed oxygen atoms of a coordinated nitrate with an interaction energy of 13.4 kJ mol^{-1} (Figure 2c). Second, two complex molecules interact with each other through several $C{-}H_{(arom)}{\bullet\bullet\bullet}O$ hydrogen bonds and one N—H•••O hydrogen bond, with an interaction energy of 133.0 kJ mol^{-1} (Figure 2d). Such an array of hydrogen bonds certainly increases the rigidity of the complexes. The formation of these hydrogen bonds is further confirmed by the Quantum

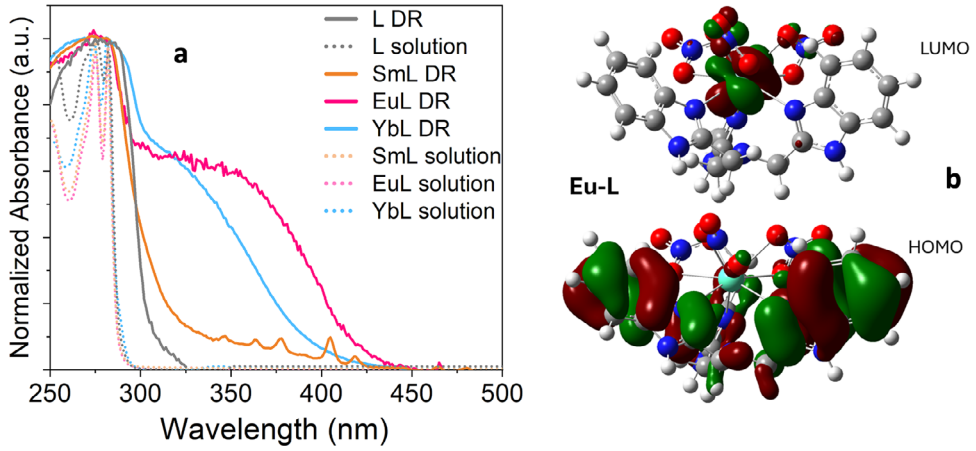

FIGURE 3 | (a) Normalized electronic absorption (dotted lines) and DR spectra (solid lines) of **EuL** (red), **YbL** (blue), **SmL** (orange), and ligand **L** (gray) in MeOH solution and in the solid state, respectively; (b) DFT-calculated HOMO and LUMO orbitals in **EuL**.

Theory of Atoms in Molecules (see Supporting Information Figure S9).

2.2 | Optical Properties

The electronic absorption spectra of the **LnL** compounds in MeOH solution and in the solid state (diffuse reflectance, DR, Figure 3a; Figure S8) are dominated by a broad and intense set of bands in the UV region (λ_{max} = 282 nm) attributed to ligand-centered transitions accompanied by a series of narrow peaks characteristic of intra-shell *f*–*f* transitions of the specific Ln ion (Figure S8b), with the only exception of the optically-silent Gd^{3+} having hardly accessible high-lying energy levels in the UV. The similarity of the spectral features of the **L** ligand in the complexes and the free form suggests a negligible influence of the coordination on its electronic properties [25]. According to Density Functional Theory (DFT) and Time Dependent-DFT (TD-DFT) calculations (Figures S10 and S11 and Table S4), the main ligand-centered absorption features are located well-below 300 nm and are attributed to singlet π–π^* transitions. Nonetheless, in the DR spectra of **EuL** and **YbL**, an additional broad band appears at longer wavelengths, and it is more redshifted in **EuL** (λ_{max} = 348 nm) than in **YbL** (λ_{max} = 316 nm). Given the isostructurality of all the complexes, this additional band cannot be ascribed to ligand-mediated supramolecular interactions, but it is clearly related to the nature of the metal ion. We attribute this optical feature to possible ligand-to-metal charge transfer (LMCT) occurring in the Eu^{3+} and Yb^{3+} complexes, in view of the fact that these ions display the highest reduction potential among the trivalent Ln ions because of the half-filled and filled configurations of their divalent species [26]. DFT calculations on **EuL** (Figure 3b) and **TbL** (Figure S12) show that, while the Highest Occupied Molecular Orbital (HOMO) is localized exclusively on the benzimidazole rings of the **L** ligand, the Lowest Unoccupied Molecular Orbital (LUMO) involves the *f*-orbitals of the Ln ion with some contribution of the coordinated nitrate ions. Even if the localization and shape of the frontier MOs are similar in the two complexes, a significantly higher energy is calculated (Table S5) for the LUMO in **TbL**, justifying the lower accessibility of this state with respect to **EuL**. These observations may corroborate the hypothesis of a possible internal CT transition occurring in **EuL** and, potentially, **YbL** complexes.

On excitation in the UV range (280 nm), all complexes, with the exception of **ErL**, exhibit the characteristic sharp *f*–*f* peaks related to the Ln ion-centered emission as shown by the photoluminescence (PL) spectra in Figure 4a–e and Figure S13. In the case of **GdL**, where no ligand-to-metal sensitization can occur, a broad ligand-centered band is detected, which peaks around 460 nm (Figure 4f). Time-resolved measurements reveal that its decay dynamics are considerably faster than in the free **L** ligand (Figure S14a). In the presence of the optically silent Gd^{3+} ion, this behavior is likely attributed to ligand singlet depopulation related to effective intersystem crossing to excited ligand triplet(s) favored by the heavy-atom effect [19, 27, 28]. Based on these observations and the PL data at 77K (Figure S14a,b), we attribute the observed emission band to residual ligand fluorescence. The excitation (PLE) spectra of the complexes (Figure S15), monitored at the wavelength of the most intense Ln-centered peak, reveal a broad band that is consistent with the absorption profile of the ligand **L**, which functions as an antenna chromophore, together with a set of narrow peaks characteristic of *f*–*f* transitions in the case of **EuL**, **TbL**, **SmL**, and **NdL**. Interestingly, for both **EuL** and **YbL**, the PLE spectra display a broad-shaped band at a lower wavelength that is coherent with the LMCT spectral profile observed in the DR spectra, thus significantly extending the spectral range for sensitized emission in these complexes. The attribution of this spectral feature to a LMCT transition is further corroborated by its significantly higher sensitivity to temperature with respect to the higher-energy ligand-centered transition (Figure S16a,b).

The time-resolved PL data (Figures S17 and S6; Table 1) indicate that all Ln ions decay monoexponentially upon indirect sensitization through the antenna ligand, in agreement with the presence of a single population of emitters. The similarity of the retrieved decay time constants in the solid state and in ACN solution indicates that the molecular structure is well-preserved when the complexes are dispersed in the solvent (Table S6). The relatively short values observed for the NIR emitters (**YbL** and **NdL**) and the absence of any detectable emission in **ErL** are likely related to the occurrence of vibrational quenching related to C—H groups

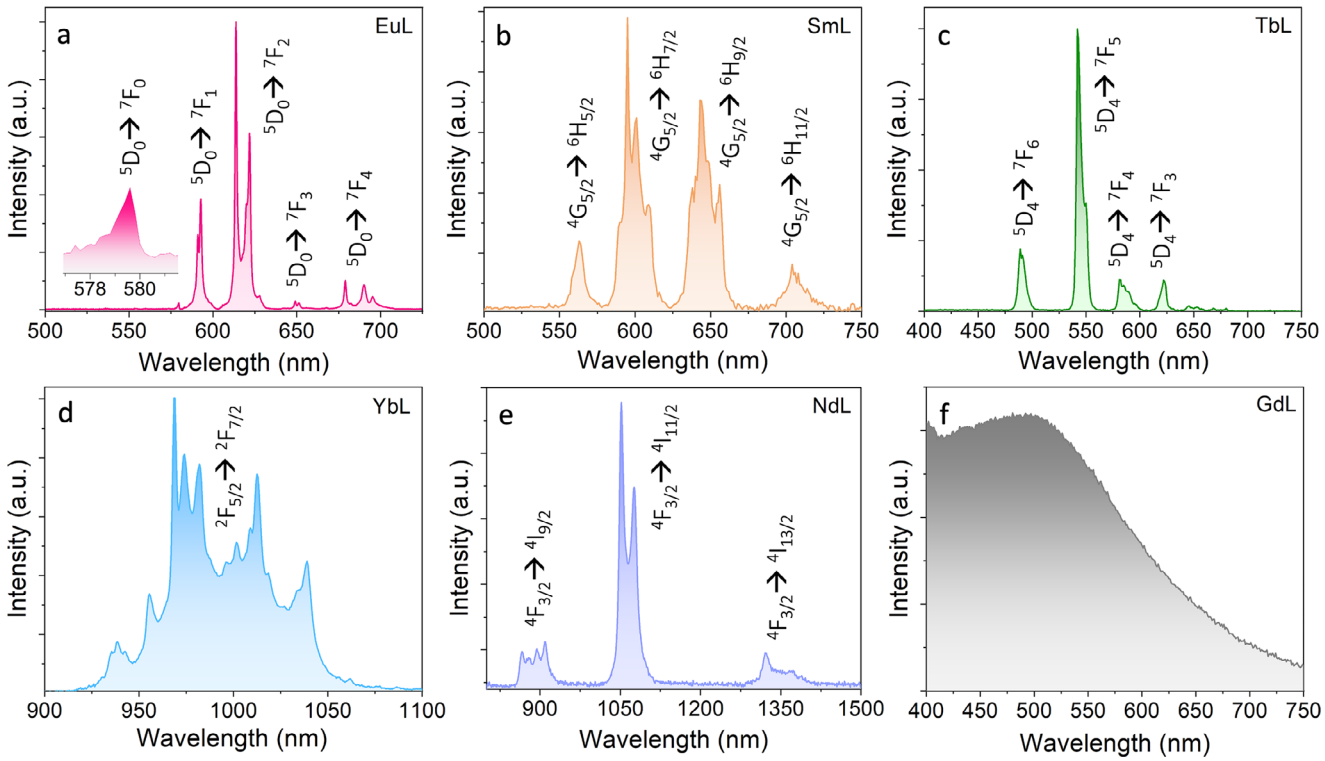

FIGURE 4 | PL spectra of LnL complexes in the crystalline state (λ_{ex} = 280 nm): (a) EuL, (b) SmL, (c) TbL, (d) YbL, (e) NdL, and (f) GdL.

TABLE 1 | Time-resolved PL data for **LnL** complexes in the solid state upon excitation at 280 nm.

Sample	λ_{em} [nm]	τ_{obs} [μs][a]
EuL	620	1250(4)
SmL	600	38.3(1)
TbL	550	1370(6)
YbL	959	4.34(1)
NdL	1064	<1

[a]τ_{obs} = observed decay time constant from monoexponential fitting.

and N—H groups in the structures of the complexes (Figure S18b and related discussion) [29]. These vibrational quenching phenomena account for the relatively small absolute quantum yield values measured in ACN solution (Tables S7 and S8).

The Ln-centered PL spectra of all the complexes display a relatively highly resolved fine structure that is coherent with the rigid and well-defined ligand field environment provided by the tetrapodal **L** ligand moiety. The PL spectrum of the **EuL** complex is particularly meaningful to retrieve information on the relationship of the optical features with the structural arrangement. As shown in Figure 3a, it displays the typical narrow lines related to the $^5D_0 \rightarrow {}^7F_J$ (J = 0–4) transitions and is dominated by an intense set of peaks around 615–630 nm, corresponding to the so-called hypersensitive electric (pseudo)quadrupolar transition $^5D_0 \rightarrow {}^7F_2$, which is considered to be highly sensitive to the local symmetry of the Eu^{3+} environment. Additionally, less intense peaks are observed around 595 nm ($^5D_0 \rightarrow {}^7F_1$), which are related to a magnetic dipole (MD)-allowed transition generally poorly influenced by the coordination environment, as well as weaker peaks in the 650–750 nm range attributed to the $^5D_0 \rightarrow {}^7F_{3\text{-}4}$ transitions. The relative intensity and fine structure of these peaks, originating from the splitting of the J sublevels of the ^7F_J term at room temperature, are coherent with the D_{4d} symmetry of the Eu^{3+} ion environment, possibly lowered by structural distortion (see Supporting Information for further discussion) [20]. Interestingly, the peak related to the purely electric dipolar (ED) $^5D_0 \rightarrow {}^7F_0$ transition, virtually prohibited by selection rules, is observed at approximately 580 nm. This transition is of particular interest in quantum information processing since it is related to non-degenerate states, and its pure ED nature makes it nearly independent of fluctuations of the magnetic field, giving rise to long optical coherence lifetime [4–6]. The origin of the appearance of this peak in Eu^{3+} molecular complexes is still subject to debate, but it is typically correlated to a low symmetry environment or J-mixing related to relatively strong crystal field effects, as corroborated by numerous studies in popular β-diketonate complexes showing particularly intense $^5D_0 \rightarrow {}^7F_0$ peaks [30, 31]. Nonetheless, low-lying CT states have also been proposed as accountable for the appearance of this transition in view of possible mixing with Eu^{3+} 4f states [20, 32]. Remarkably, this latter circumstance seems herein the most likely given the above considerations about the presence of an LMCT transition in the absorption spectrum of **EuL**. To further elucidate this point, we retrieved the Eu^{3+} radiative lifetime (τ_{rad}) through Einstein's equation for spontaneous emission, which basically depends on the ratio between the integrated intensity of the PL spectrum and the intensity of the environment-independent MD $^5D_0 \rightarrow {}^7F_1$ band [33]. The retrieved value of τ_{rad} = 2.99 ms, which increases to 4.66 ms at 77 K (Figure S19), is indicative of a weaker crystal field and a higher symmetry environment with respect to archetype β-diketonate complexes such as $Eu(BTFA)_3(H_2O)_2$

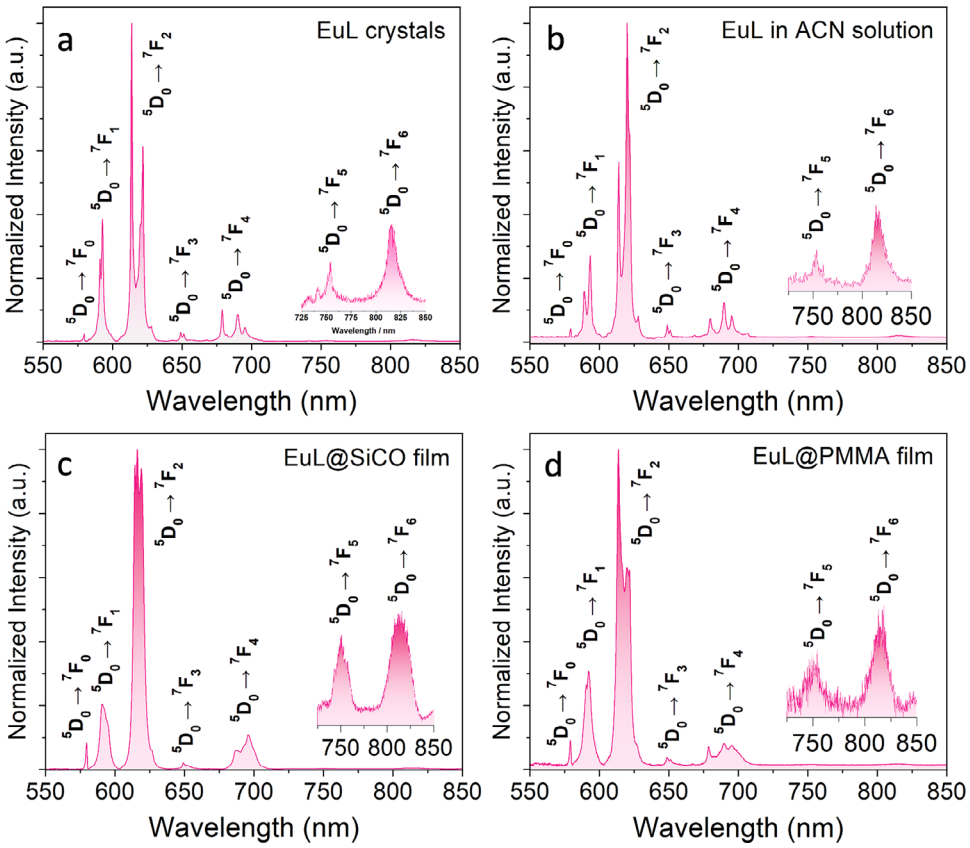

FIGURE 5 | PL spectra (λ_{ex} = 280 nm) of **EuL** in the solid state (a), in ACN solution (b), and in doped SiCO (c) and PMMA (d) matrix. Optical bandpass was 0.1 nm.

(τ_{rad} = 1.61 ms, Figure S20) and [Eu(DBM)$_3$Phen] (τ_{rad} = 0.80 ms) [31] (BTFA = benzoyltrifluoro acetonate; DBM = dibenzoyl methanoate) showing detectable $^5D_0 \rightarrow {}^7F_0$ transitions. Moreover, it is interesting to note that the intensity and width of the $^5D_0 \rightarrow {}^7F_0$ peak in **EuL** is unchanged when lowering the temperature to 77 K, even if phonon suppression likely leads to a symmetry increase, as suggested by the observed increase of the radiative lifetime (Figure S19). These observations point out the possible role of the LMCT state, rather than local symmetry, in enhancing this peak in **EuL**, allowing for its appearance also in a highly rigid environment, which certainly is a favorable requisite to reduce optical decoherence.

While the described structural and optical properties indeed make **EuL** a promising material for molecular quantum light sources, the exploration of its processing potential for on-chip integrated devices and the study of the influence of host platforms on its spectral features are imperative for practical applications. We therefore doped **EuL** into dielectric and optically transparent media, suitable to be combined with metal mirror cavities for optical signal coherent enhancement and acting as spacers between the emitter and the metal surface to avoid metal quenching. We selected the silica-based SiCO polymeric matrix (Figures S22–S24), which yields mechanically flexible and shrinkage-resistant films thanks to the long alkyl chains of the castor oil co-precursor [34], along with the highly popular PMMA (polymethyl-methacrylate) polymer host, to afford doped **EuL@SiCO** and **EuL@PMMA** films (~1 mm thick, 1 % wt.). Figure 5 shows a comparison of the extended PL spectra (550–850 nm) of **EuL** in different phases, as crystals, in acetonitrile (ACN) solution, as well as in SiCO and PMMA doped films, while Tables S9 and S10 report the retrieved values of oscillator strengths and branching ratios for the $^5D_0 \rightarrow {}^7F_J$ transitions of Eu^{3+}. It is noteworthy that we were also able to detect the weak $^5D_0 \rightarrow {}^7F_5$ (~750 nm) and $^5D_0 \rightarrow {}^7F_6$ (~850 nm) peaks, rarely reported in the literature, for every phase investigated. This latter transition is particularly relevant to retrieve some specific information about the rigidity of the emitter's environment, as discussed later. Table 2 summarizes the main photophysical data from time-resolved PL measurements.

TABLE 2 | Photophysical data for **EuL** in different phases.

Sample	κ_{rad} [s^{-1}][a]	τ_{rad} [ms]	τ_{obs} [ms][b]	ϕ_{Eu} [%][c]
Crystals	282	2.99	1.250(4)	42
ACN solution	425	2.48	1.171(3)	47
EuL@SiCO	410	2.40	1.089(8)	45
EuL@PMMA	353	2.81	0.290(1)	10

[a] $\kappa_{rad} = 1/\tau_{rad}$, radiative rate.
[b] τ_{obs} values obtained from monoexponential fitting of decay curves for the samples Crystals, ACN solution and **EuL@SiCO**. In the case of **EuL@PMMA** the reported value refers to the intensity average lifetime ($\tau_{av} = \Sigma a_i \tau_i^2 / \Sigma a_i \tau_i$; a, amplitude) from biexponential fitting.
[c] $\phi_{Eu} = \tau_{obs}/\tau_{rad}$, Eu^{3+} intrinsic quantum yield.

TABLE 3 | Experimental Judd–Ofelt parameters (Ω_l) and asymmetric ratio ($R_{2/1}$) for **EuL** complex in the crystalline state, ACN solution, and incorporated into SiCO or PMMA matrices.

Sample	Ω_2 (10^{-20} cm^2)	Ω_4 (10^{-20} cm^2)	Ω_6 (10^{-20} cm^2)	$R_{2/1}$
Crystals	5.95	2.32	2.52	3.35
ACN solution	8.64	3.38	4.27	4.82
EuL@SiCO	10.22	3.37	1.32	5.77
EuL@PMMA	7.53	2.39	1.21	4.24

As expected, a loss of the spectral fine structure resolution is observed when **EuL** is dispersed in solution, which is more accentuated in the doped polymeric films as a consequence of increased inhomogeneous line broadening due to phonon effects and possible local distortion related to the interaction with the matrix. This observation is supported by the observed decrease of the radiative lifetime with respect to the crystalline state, as reported in Table 2. On the other hand, in solution and in the doped SiCO film, the retrieved decay times from monoexponential fitting only slightly differ from the value observed in the crystalline state, suggesting that the structure of the complex is well preserved and its rigid nature protects the Eu^{3+} emitter from external detrimental quenching effects by the solvent and polymer host. Remarkably, the $^5D_0 \rightarrow {}^7F_0$ peak remains detectable in all phases and is even enhanced in intensity in both **EuL@SiCO** and **EuL@PMMA**. It is interesting to note that the LMCT band is still visible in the PLE spectra of **EuL** and **YbL** in solution and in the SiCO film (Figure S25), and it may still be accountable for the appearance of the $^5D_0 \rightarrow {}^7F_0$ transition line. This also represents strong evidence that the molecular structure is preserved upon dispersion in solution or in the polymer matrix. To further investigate the role of host interactions in shaping the optical properties of **EuL**, we applied the Judd–Ofelt formalism to retrieve information about the local environment of the Eu^{3+} emitter, including its symmetry, polarizability, and rigidity [35, 36].

The Judd–Ofelt parameters of the **EuL** complex in ACN solution, in the solid state, and incorporated into SiCO and PMMA matrices were calculated using LUMPAC 2.0 [37] software and are summarized in Table 3. The Ω_2 values increase upon incorporation into the PMMA and SiCO matrices, indicating insertion into a more polarizable environment and a decrease in the local symmetry around the Eu^{3+} ion, which is directly correlated to the observed enhancement of the hypersensitive $^5D_0 \rightarrow {}^7F_2$ transition, consistent with the increasing trend of the $R_{2/1}$ ($= I(^5D_0 \rightarrow {}^7F_2)/I(^5D_0 \rightarrow {}^7F_1)$) ratios on going from the crystalline state to the SiCO film. In solution, Ω_2 is also raised, suggesting possible solvent-induced distortion and vibrational effects partially disrupting the symmetry. However, the retrieved values are significantly lower than those typically found in β-diketonate complexes [38, 39], indicating a higher symmetry of the coordination environment in **EuL**, which is overall well preserved even upon incorporation into the films. This observation is particularly relevant when considering that hypersensitivity (to which Ω_2 is directly related) can be associated with an inhomogeneous distribution of oscillating electric dipoles related to the surrounding ligand system, which can strongly interact with the pseudo-quadrupolar (and ED) 4*f* transitions [40]. Therefore, the reduced Ω_2 value observed in **EuL**, indicating reduced electric inhomogeneity, is again a favorable factor for limiting the decoherence of quantum light from the Eu^{3+} emitter. The Ω_4 values can be grouped into two sets: ACN solution and SiCO film, which exhibit higher values, and crystals and PMMA film, which show lower ones. Although the physical meaning of this parameter is not fully understood, we can tentatively rationalize the increase in Ω_4 in terms of shorter Eu–ligand bond distances, suggesting stronger interactions of the complex with ACN and SiCO compared to PMMA, where the Ω_4 value remains similar to that of the crystalline phase [41, 42]. Finally, the Ω_6 parameter, which is related to the rigidity of the system, follows the expected trend: it decreases progressively from solution to crystals and then to the polymeric films, reflecting the increasing rigidity of the surrounding medium. The SiCO and PMMA doped films exhibit comparable Ω_6 values, evidencing an equivalent rigidity effect of the SiCO matrix over the immediate surroundings, and hence spectral features, of Eu^{3+}, despite its significantly higher mechanical flexibility with respect to PMMA [43]. System rigidity is important to reduce inhomogeneous line broadening, a crucial aspect to achieve potential quantum light sources for optical quantum information storage applications. Therefore, we inspected the full widths at half-maximum (FWHM) of the purely ED $^5D_0 \rightarrow {}^7F_0$ transition peak for **EuL** in the different phases at room temperature, which are summarized in Figure 6. While the presence of a single peak again confirms that the molecular structure of the complex is fully preserved when dispersed in the solvent or in the polymer hosts, the FWHM value is indicative of the small fluctuations of the surrounding environment of Eu^{3+} sites across the material, possibly due to small distortions related to phonon effects or interactions with the matrix. It can be noticed that the retrieved values in the SiCO (~31 cm^{-1}) and PMMA films (~26 cm^{-1}) only increase by less than 70 % with respect to the value obtained in the single crystals (~18 cm^{-1}). These values are much smaller than those found for Eu^{3+} in glasses (in the range 100–150 cm^{-1}) [44, 45], underlining the potential superiority of rationally designed Ln molecular complexes over traditional inorganic materials for optical quantum applications. Moreover, the high rigidity imposed by the tetrapodal **L** ligand leads to a reduced linewidth with respect to the bidentate β-diketonate complexes (Figure S21). Remarkably, while the observed inhomogeneous linewidths of about 500 and 900 GHz in the crystals and in the polymeric hosts at room temperature are higher than the few tens of GHz measured for Eu^{3+} doped in inorganic hosts (150 GHz) [46] or in molecular complexes (<100 GHz) [4–6] at cryogenic temperatures (< 4.2 K), they are lower than the thousands of GHz found for the conventional terrylene molecular quantum emitters doped into polymer hosts [3, 47]. These figures of merit, which are favorable for the exploitation of **EuL** as a promising source

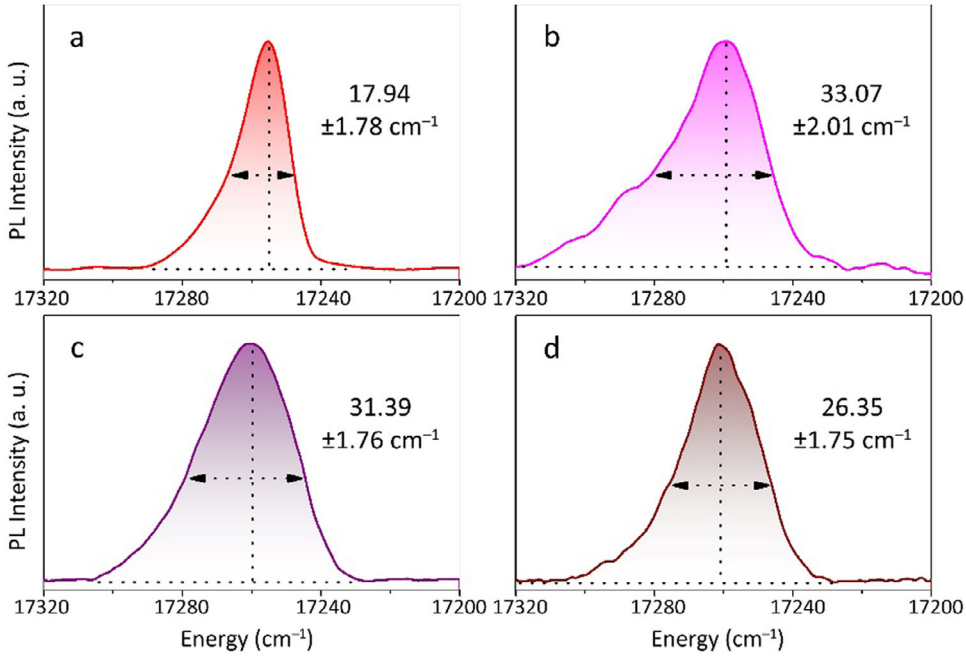

FIGURE 6 | Comparison of the PL spectral shape of the purely ED $^5D_0 \rightarrow {}^7F_0$ transition peak for **EuL** in different phases at room temperature: (a) crystals; (b) ACN solution; (c) **EuL@SiCO**; (d) **EuL@PMMA**. The retrieved FHWM values and related uncertainties are indicated (details in Supporting Information). Optical bandpass was 0.1 nm.

of highly coherent light in quantum devices, likely stem from the highly rigid molecular structure and the described peculiar electronic properties of the **L** ligand.

2.3 | Color-Tunable SiCO Films

The observed excitation wavelength-dependent PL properties of the visible-emitting **EuL** and **TbL** complexes (Figure S25b), combined with the intrinsic optical features of the SiCO polymer host, bestow notable color-tunability properties on the doped films, which can be of interest in various optical applications, such as anticounterfeiting and optical multiplexing. As shown in Figure S23, the undoped SiCO film displays broad emission in the blue region of the visible spectral range (λ_{max} = 478 nm) upon excitation in the 300–370 nm region [32]. From the comparison with the PLE spectra of **EuL@SiCO** and **Tb@SiCO** in Figure S25b, it becomes evident that the **SiCO** excitation range is only partially overlapping with that of **TbL**, which is significantly blueshifted, while it overcomes the intensity of the LMCT band for **EuL** because of the concentration mismatch between the polymer host and the doped complex. As a result, the excitation–emission maps of **EuL@SiCO** and **TbL@SiCO** materials, reported in Figure 7a,b, respectively, reveal a strong dependence of the emission profile and perceived color on the excitation wavelength. In the **EuL@SiCO** sample, excitation in the 260–290 nm range selectively enhances the characteristic red emission bands of Eu^{3+}, resulting in a saturated red chromaticity. As the excitation wavelength regularly increases, subtle shifts in the relative intensities of Eu^{3+}-centered and SiCO emission peaks induce variations in the emitted color (Figure 7c,d), as confirmed by the corresponding displacement of coordinates in the CIE chromaticity diagram (inset in Figure 7a), where excitation at the longest wavelengths (330–400 nm) results in a purple emission color stemming from the combination of the simultaneously-excited red and blue components of Eu^{3+} and the SiCO polymer. Conversely, upon selective irradiation in the 260–290 nm range, the **TbL@SiCO** sample exhibits intense green emission dominated by the 545 nm transition (Figure 7e). This green emission is strongly quenched at higher excitation wavelengths, where the emission of the SiCO polymer host becomes predominant, yielding blue emission (Figure 7f). The observed excitation-dependent shift in the emission profiles of the **LnL@SiCO** films underscores the role of ligand-to-metal charge transfer and host–sensitization processes in governing the photophysical behavior, enabling tunable color output through selective excitation. It is worth underlining that the negligible autofluorescence of the SiCO matrix upon irradiation at wavelengths below 300 nm is extremely advantageous to the removal of the background interference typically observed in several optical applications, including quantum photonics, involving luminescent materials doped in a polymer host, commonly PMMA [48].

Upon prolonged UV irradiation at 333 nm, **EuL@SiCO** exhibited nearly unchanged photoluminescence for over 2 h of illumination time, followed by a gradual reduction of the overall photoluminescence intensity attributed to progressive photochemical reactions such as ligand oxidation, polymer backbone degradation, or disruption of the Eu^{3+} coordination environment, as illustrated in Figure 7g. However, the emission intensity stabilized after about 5 h at roughly 55 %–60 % of the initial value, indicating that a portion of the luminescent centers remains intact and that the system reaches a quasi-equilibrium state where further degradation proceeds at a significantly slower rate. Interestingly, the chromaticity diagrams (CIE 1931) reveal a concurrent shift in emission coordinates over time, consistent with alterations

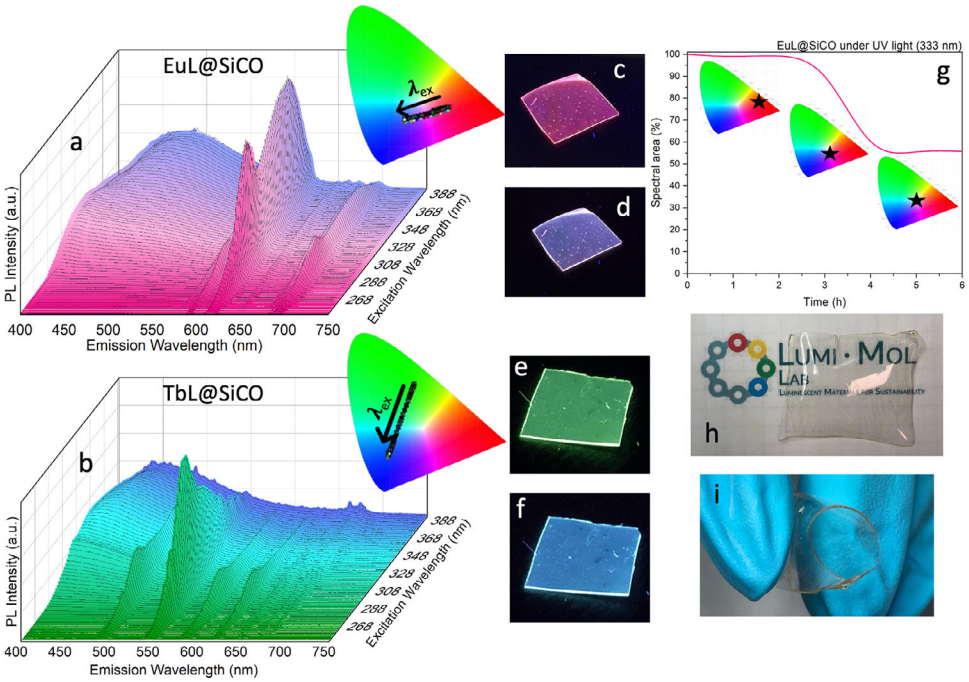

FIGURE 7 | 3D excitation-dependent emission maps (λ_{ex} = 250–400 nm) of **EuL@SiCO** 1 % (a) and **TbL@SiCO** 0.5 %. (b) Corresponding 2D maps are reported in Figure S24. Photographs of **EuL@SiCO** under UV light (c), λ_{ex} = 280 nm; (d), λ_{ex} = 365 nm, and under white light, (h) and (i); Photographs of **TbL@SiCO** under UV light (e), λ_{ex} = 280 nm; (f), λ_{ex} = 365 nm; (g) Time-dependent variation in spectral area and emission color upon continuous UV irradiation of **EuL@SiCO** (λ_{ex} = 333 nm) with corresponding CIE1931 chromaticity diagrams.

in the spectral distribution, leading to almost pure white light generation (CIE coordinates x = 0.36, y = 0.33) at long exposure times.

3 | Conclusion

In conclusion, we investigated the synthesis and the structure-properties relationship of a series of luminescent Ln complexes with the tris-benzimidazolic **L** ligand to be proposed as potential coherent quantum light sources. In the complexes, the **L** ligand coordinates the metal center in a tetrapodal fashion, where the coordination sphere is completed by three chelating nitrate ions. This molecular arrangement, together with an extended network of intramolecular hydrogen bonds in the crystalline state, affords a highly rigid molecular structure. As a result, the Ln-centered emission spectral profiles, obtained upon photoexcitation in the ligand absorption band, show a particularly well-resolved fine structure with narrow lines related to the *J* sublevels of the 4*f* levels. In particular, the photoluminescence spectrum of the europium **EuL** derivative displays the appearance of a single line related to the purely electric dipolar $^5D_0 \rightarrow {}^7F_0$ transition, which is of high interest in quantum photonics applications due to its intrinsic long optical coherence lifetime. Remarkably, we found that the origin of this line, which is formally prohibited by selection rules, may be related to the occurrence of a LMCT state, taking place solely in the europium and ytterbium complexes, rather than to the typically accounted low symmetry or strong crystal field effects. Importantly, this mechanism allows for the appearance of the $^5D_0 \rightarrow {}^7F_0$ band while observing low hypersensitivity, as demonstrated by Judd-Ofelt calculations, indicating a limited electric inhomogeneity of the ligand system. Moreover, thanks to the high rigidity of the coordination environment, the inhomogeneous linewidth (~500 GHz) at room temperature is significantly reduced with respect to that of the zero-phonon lines of polyaromatic hydrocarbon molecules in polymer hosts, traditionally investigated as molecular single photon emitters. These figures of merit, which are largely maintained when **EuL** is incorporated into transparent polymer silica-based (SiCO) and PMMA films, are favorable for limiting the decoherence of quantum light from the Eu^{3+} emitter. Finally, the high excitation selectivity of the highly transparent and flexible SiCO films doped with **EuL** and **TbL** complexes allows for avoiding the interfering background autofluorescence of the host in photonics applications. At the same time, it delivers wide color tunability of the emission upon changing the excitation wavelength, which can be exploited in several fields such as anti-counterfeiting. This study highlights the importance of molecular engineering for a rational design of Ln-based quantum light sources and opens novel, promising pathways for their on-chip integration.

[CCDC 2505974–2505975 contains the supplementary crystallographic data for this paper. These data can be obtained free of charge from The Cambridge Crystallographic Data Centre via www.ccdc.cam.ac.uk/data_request/cif].

Acknowledgements

This work received support from the European Innovation Council under the Horizon Europe framework programme through a HORIZON-EIC-2022-PATHFINDERCHALLENGES-01-06 project "ARTEMIS – *Molecular Materials for on-chip integrated quantum light sources*" – GA n. 101115149. We also acknowledge financial support under the National Recovery and

Resilience Plan (NRRP), Mission 4, Component 2, Investment 1.1, Call for tender No. 104 published on 2.2.2022 by the Italian Ministry of University and Research (MUR), funded by the European Union – Next Generation EU– Project Title "QuantaMol—*Molecular Quantum Light Sources*" – CUP C53D23007330001- Grant Assignment Decree No. 1380 adopted on 01-09-2023 by the Italian Ministry of University and Research (MUR).

Open access publishing facilitated by Universita degli Studi del Piemonte Orientale Amedeo Avogadro, as part of the Wiley - CRUI-CARE agreement.

Funding

This work received support from the European Innovation Council under the Horizon Europe framework programme through a HORIZON-EIC-2022-PATHFINDERCHALLENGES-01-06 project "ARTEMIS – *Molecular Materials for on-chip integrated quantum light sources*" – GA n. 101115149 and from the Italian Ministry of University and Research (MUR) under the National Recovery and Resilience Plan (NRRP) funded by the European Union Next Generation EU through the project "QuantaMol - Molecular Quantum Light Sources" CUP C53D23007330001.

Conflicts of Interest

The authors declare no conflicts of interest.

Data Availability Statement

The data that support the findings of this study are available from the corresponding author upon reasonable request.

References

1. S. Bogdanov, M. Y. Shalaginov, A. Boltasseva, and V. M. Shalaev, "Material Platforms for Integrated Quantum Photonics," *Optical Materials Express* 7 (2017): 111–132, https://doi.org/10.1364/OME.7.000111.

2. G. Yang, Z. Li, and K. Wu, "Periodically Poled Monolayer Lithium Niobate for Photonic Chips of Quantum Devices," *ACS Applied Optical Materials* 1 (2023): 115–122, https://doi.org/10.1021/acsaom.2c00015.

3. C. Toninelli, I. Gerhardt, A. S. Clark, et al., "Single Organic Molecules for Photonic Quantum Technologies," *Nature Materials* 20 (2021): 1615–1628, https://doi.org/10.1038/s41563-021-00987-4.

4. K. S. Kumar, D. Serrano, A. M. Nonat, et al., "Optical Spin-State Polarization In A Binuclear Europium Complex Towards Molecule-Based Coherent Light-Spin Interfaces," *Nature Communications* 12 (2021): 2152, https://doi.org/10.1038/s41467-021-22383-x.

5. D. Serrano, S. K. Kuppusamy, B. Heinrich, et al., "Ultra-Narrow Optical Linewidths In Rare-Earth Molecular Crystals," *Nature* 603 (2022): 241–246, https://doi.org/10.1038/s41586-021-04316-2.

6. S. K. Kuppusamy, E. Vasilenko, W. Li, et al., "Observation of Narrow Optical Homogeneous Linewidth and Long Nuclear Spin Lifetimes in a Prototypical [Eu(trensal)] Complex," *The Journal of Physical Chemistry C* 127 (2023): 10670–10679, https://doi.org/10.1021/acs.jpcc.3c02903.

7. L. R. Weiss, G. T. Smith, R. A. Murphy, et al., "A High-Resolution Molecular Spin-Photon Interface At Telecommunication Wavelengths," *Science* 390 (2025): 76–81, https://doi.org/10.1126/science.ady8677.

8. B. C. Buchler, T. Kalkbrenner, C. Hettich, and V. Sandoghdar, "Measuring the Quantum Efficiency of the Optical Emission of Single Radiating Dipoles Using a Scanning Mirror," *Physical Review Letters* 95 (2005): 063003, https://doi.org/10.1103/PhysRevLett.95.063003.

9. D. Wang, H. Kelkar, D. M. Cano, et al., "Turning a Molecule Into a Coherent Two-Level Quantum System," *Nature Physics* 15 (2019): 483–489, https://doi.org/10.1038/s41567-019-0436-5.

10. R. Lettow, Y. L. A. Rezus, A. Renn, et al., "Quantum Interference of Tunably Indistinguishable Photons From Remote Organic Molecules," *Physical Review Letters* 104 (2010): 123605, https://doi.org/10.1103/PhysRevLett.104.123605.

11. J. B. Trebbia, P. Tamarat, and B. Lounis, "Indistinguishable Near-Infrared Single Photons From an Individual Organic Molecule," *Physical Review A* 82 (2010): 063803, https://doi.org/10.1103/PhysRevA.82.063803.

12. T. Basché, W. E. Moerner, M. Orrit, and H. Talon, "Photon Antibunching in the Fluorescence of Single Dye Molecule Trapped in a Solid," *Physical Review Letter* 69 (1992): 1516–1519.

13. P. Lombardi, A. P. Ovvyan, S. Pazzagli, et al., "Photostable Molecules on Chip: Integrated Sources of Nonclassical Light," *ACS Photonics* 5 (2018): 126–132, https://doi.org/10.1021/acsphotonics.7b00521.

14. C. Toninelli, K. Early, J. Bremi, A. Renn, S. Götzinger, and V. Sandoghdar, "Near-Infrared Single-Photons From Aligned Molecules in Ultrathin Crystalline Films at Room Temperature," *Optics Express* 18 (2010): 6577–6582, https://doi.org/10.1364/OE.18.006577.

15. M. Takaishi, T. Komino, A. Kameda, et al., "Suppression Of The Plasmon-Quenching Effect On Light Amplification in 20-μm-Diameter Plasmonic Whispering Gallery Mode Resonators Fabricated From Bowl-Shaped Organic/Metal Thin Films," *Physical Chemistry Chemical Physics* 26 (2024): 10796–10803, https://doi.org/10.1039/D4CP00389F.

16. T. Zhong and P. Goldner, "Emerging Rare-Earth Doped Material Platforms For Quantum Nanophotonics," *Nanophotonics* 8, no. 11 (2019): 2003–2015, https://doi.org/10.1515/nanoph-2019-0185.

17. K. Huang, J. Fung-A-Fat, J. Wu, et al., "Lanthanide-Based Quantum Optical Materials," *Advanced Functional Materials* (2025): 24562, https://doi.org/10.1002/adfm.202524562.

18. A. J. Shin, C. Zhao, Y. Shen, et al., "Toward Liquid Cell Quantum Sensing: Ytterbium Complexes With Ultranarrow Absorption," *Science* 385 (2024): 651–656, https://doi.org/10.1126/science.adf7577.

19. F. Quochi, M. Saba, F. Artizzu, et al., "Ultrafast Dynamics of Intersystem Crossing and Resonance Energy Transfer in Er(III)−Quinolinolate Complexes," *The Journal of Physical Chemistry Letters* 1 (2010): 2733–2737, https://doi.org/10.1021/jz101044d.

20. K. Binnemans, "Interpretation of Europium(III) Spectra," *Coordination Chemistry Reviews* 295 (2015): 1–45, https://doi.org/10.1016/j.ccr.2015.02.015.

21. F. Artizzu, L. Marchiò, M. L. Mercuri, et al., "New Insights on Near-Infrared Emitters Based on Er-quinolinolate Complexes: Synthesis, Characterization, Structural, and Photophysical Properties," *Advanced Functional Materials* 17 (2007): 2365–2376, https://doi.org/10.1002/adfm.200600926.

22. S. Goswami, S. Biswas, K. Tomar, and S. Konar, "Tuning the Magnetoluminescence Behavior of Lanthanide Complexes Having Sphenocorona and Cubic Coordination Geometries," *European Journal of Inorganic Chemistry* 2016 (2016): 2774–2782, https://doi.org/10.1002/ejic.201600152.

23. J. J. Jiang, M. Pan, J. M. Liu, W. Wang, and C. Y. Su, "Assembly of Robust and Porous Hydrogen-Bonded Coordination Frameworks: Isomorphism, Polymorphism, and Selective Adsorption," *Inorganic Chemistry* 49 (2010): 10166–10173, https://doi.org/10.1021/ic1014384.

24. G. R. Desiraju, J. J. Vittal, and A. Ramanan, *Crystal Engineering* (World Scientific Publishing, 2011).

25. M. Pan, X.-L. Zheng, Y. Liu, W.-S. Liu, and C.-Y. Su, "Structural and Photoluminescent Studies Of Lanthanide Complexes With Tripodal triRNTB (N-substituted tris(benzimidazol-2-ylmethyl)amine): Ligand Substituent, Anionic And Secondary Ligand Effects," *Dalton Transactions* (2009): 2157–2169, https://doi.org/10.1039/B818322H.

26. W. D. Horrocks Jr., J. P. Bolender, W. D. Smith, and R. M. Supkowski, "Photosensitized Near Infrared Luminescence of Ytterbium(III) in Proteins and Complexes Occurs via an Internal Redox Process," *Journal of the American Chemical Society* 119 (1997): 5972–5973, https://doi.org/10.1021/ja964421l.

27. J. Liu, P. Geiregat, L. Pilia, R. Van Deun, and F. Artizzu, "Molecular Size Matters: Ultrafast Dye Singlet Sensitization Pathways to Bright Nanoparticle Emission," *Advanced Optical Materials* 9 (2021): 2001678, https://doi.org/10.1002/adom.202001678.

28. F. Artizzu, F. Quochi, L. Marchiò, et al., "Light Conversion Control in NIR-Emissive Optical Materials Based on Heterolanthanide Er_xYb_{3-x} Quinolinolato Molecular Components," *Chemistry of Materials* 27, no. 11 (2015): 4082–4092, https://doi.org/10.1021/acs.chemmater.5b01109.

29. D. Mara, F. Artizzu, P. F. Smet, A. M. Kaczmarek, K. Van Hecke, and R. Van Deun, "Vibrational Quenching in Near-Infrared Emitting Lanthanide Complexes: A Quantitative Experimental Study and Novel Insights," *Chemistry—A European Journal* 25 (2019): 15944–15956, https://doi.org/10.1002/chem.201904320.

30. A. F. Kirby and F. S. Richardson, "Detailed Analysis Of The Optical Absorption And Emission Spectra Of Europium(3+) in the Trigonal (C3) Eu(DBM)3.H2O System," *The Journal of Physical Chemistry* 87, no. 14 (1983): 2544–2556, https://doi.org/10.1021/j100237a018.

31. J.-S. Kang, Y.-K. Jeong, Y.-S. Shim, S. Rout, and K. T. Jung, "Structures, And Luminescence And Magnetic Properties of Ln() Complexes Bearing Dibenzoylmethane Ligand (Ln=Eu and Gd)," *Journal of Luminescence* 178 (2016): 368–374, https://doi.org/10.1016/j.jlumin.2016.06.008.

32. X. Y. Chen and G. K. Liu, "The Standard And Anomalous Crystal-Field Spectra of Eu^{3+}," *Journal of Solid State Chemistry* 178, no. 2 (2005): 419–428, https://doi.org/10.1016/j.jssc.2004.09.002.

33. M. H. V. Werts, R. T. F. Jukes, and J. W. Verhoeven, "The Emission Spectrum And The Radiative Lifetime of Eu^{3+} in Luminescent Lanthanide Complexes," *Physical Chemistry Chemical Physics* 4 (2002): 1542–1548, https://doi.org/10.1039/B107770H.

34. B. Damasio de Freitas, B. S. Domingos Onishi, F. J. Caixeta, et al., "Green Host Urethanesil Based On Castor Oil Doped With Eu^{3+} Complex," *Optical Materials* 138 (2023): 113706, https://doi.org/10.1016/j.optmat.2023.113706.

35. B. R. Judd, "Optical Absorption Intensities of Rare-Earth Ions," *Physical Review* 127 (1962): 750–761, https://doi.org/10.1103/PhysRev.127.750.

36. G. S. Ofelt, "Intensities of Crystal Spectra of Rare-Earth Ions," *The Journal of Chemical Physics* 37 (1962): 511–520, https://doi.org/10.1063/1.1701366.

37. J. D. L. Dutra, W. F. Oliveira, G. S. Silva, T. D. Bispo, and R. O. Freire, "LUMPAC 2.0—Bridging Theory and Experiment in the Study of Luminescent Systems," *Journal of Computational Chemistry* 46, no. 17 (2025): 70143, https://doi.org/10.1002/jcc.70143.

38. C. C. L. Pereira, S. Dias, I. Coutinho, J. P. Leal, L. C. Branco, and C. A. T. Laia, "Europium(III) Tetrakis(β-Diketonate) Complex as an Ionic Liquid: A Calorimetric and Spectroscopic Study," *Inorganic Chemistry* 52 (2013): 3755–3764, https://doi.org/10.1021/ic3023024.

39. Y. Luo, B. Chen, W. Wu, X. Yu, Q. Yan, and Q. Zhang, "Judd–Ofelt Treatment On Luminescence Of Europium Complexes With β-diketone and bis(β-diketone)," *Journal of Luminescence* 129 (2009): 1309–1313, https://doi.org/10.1016/j.jlumin.2009.06.016.

40. C. K. Jørgensen and B. R. Judd, "Hypersensitive Pseudoquadrupole Transitions in Lanthanides," *Molecular Physics* 8, no. 3 (1964): 281–290, https://doi.org/10.1080/00268976400100321.

41. R. Devi, S. Chahar, S. P. Khatkar, V. B. Taxak, and P. Boora, "Relative Study of Luminescent Properties With Judd-Ofelt Characterization in Trivalent Europium Complexes Comprising ethyl-(4-fluorobenzoyl) Acetate," *Journal of Fluorescence* 27, no. 4 (2017): 1349–1358, https://doi.org/10.1007/s10895-017-2069-3.

42. A. Hooda, D. Singh, A. Dalal, et al., "Preparation, Spectral and Judd Ofelt Analyses of Luminous Octa-Coordinated Europium (III) Complexes," *Journal of Photochemistry and Photobiology A: Chemistry* 440 (2023): 114646, https://doi.org/10.1016/j.jphotochem.2023.114646.

43. E. A. Lalla, M. Konstantinidis, I. De Souza, et al., "Judd-Ofelt parameters of RE^{3+}-doped fluorotellurite glass (RE^{3+}= Pr^{3+}, Nd^{3+}, Sm^{3+}, Tb^{3+}, Dy^{3+}, Ho^{3+}, Er^{3+}, and Tm^{3+})," *Journal of Alloys and Compounds* 845 (2020): 156028, https://doi.org/10.1016/j.jallcom.2020.156028.

44. V. Lavín, U. R. Rodríguez-Mendoza, I. R. Martín, and V. D. Rodríguez, "Optical Spectroscopy Analysis of the Eu^{3+} Ions Local Structure In Calcium Diborate Glasses," *Journal of Non-Crystalline Solids* 319, no. 1–2 (2003): 200–216, https://doi.org/10.1016/S0022-3093(02)01914-2.

45. R. Reisfeld, R. A. Velapoldi, L. Boehm, and M. Ish-Shalom, "Transition Probabilities of Europium in Phosphate Glasses," *The Journal of Physical Chemistry* 75, no. 26 (1971): 3980–3983, https://doi.org/10.1021/j100695a012.

46. F. Konz, Y. Sun, C. W. Thiel, et al., "Temperature And Concentration Dependence Of Optical Dephasing, Spectral-Hole Lifetime, And Anisotropic Absorption in Eu^{3+}:Y_2SiO_5," *Physical Review B* 68 (2003): 085109, https://doi.org/10.1103/PhysRevB.68.085109.

47. M. Orrit, J. Bernard, A. Zumbusch, and R. I. Personov, "Stark Effect on Single Molecules in a Polymer Matrix," *Chemical Physics Letters* 196, no. 6 (1992): 595–600, https://doi.org/10.1016/0009-2614(92)86000-8.

48. E. Ellingwood, H. Benmansour, Q. Hars, et al., "Ultraviolet-Induced Fluorescence of poly(methyl methacrylate) Compared to 1,1,4,4-tetraphenyl-1,3-butadiene Down to 4 K," *Nuclear Instruments and Methods in Physics Research Section A: Accelerators, Spectrometers, Detectors and Associated Equipment* 1039 (2022): 167119, https://doi.org/10.1016/j.nima.2022.167119.

Supporting Information

Additional supporting information can be found online in the Supporting Information section.

Supporting File: adom71071-sup-0001-SuppMat.pdf.